Backscattering-immune optomechanical entanglement in a whispering-gallery-mode resonator

Bo Zhao,[1,2] Mei-Rong Wei,[1,2] and Qi Guo[1,2,*]

[1] *State Key Laboratory of Quantum Optics and Quantum Optics Devices, Institute of Opto-Electronics, College of Physics and Electronic Engineering, Shanxi University, Taiyuan, Shanxi 030006, China*

[2] *Collaborative Innovation Center of Extreme Optics, Shanxi University, Taiyuan 030006, China*

(Received 31 July 2024; revised 5 November 2024; accepted 28 January 2025; published 24 February 2025)

We propose how to achieve a backscattering-immune quantum system containing a cavity with defects. We find that, by placing a nanoparticle in the evanescent field of the whispering-gallery-mode resonator with proper relative position and size, the impact of backscattering induced by the defect can be almost eliminated completely. This makes it possible to realize backscattering immunity for both quantum entanglement and classical information transmission. We also show that both the degree of optomechanical entanglement and the transmissivity of the resonator can be manipulated by tuning the relative position of the nanoparticle. This work provides insights into the protection and manipulation of quantum and classical resources, which is meaningful for building noise-tolerant optomechanical quantum processors, achieving ideal quantum precision measurements and backscattering-immune integrated quantum photonic circuits.

DOI: 10.1103/PhysRevApplied.23.024061

I. INTRODUCTION

Quantum entanglement, the "spooky" feature of quantum mechanics, is one of the most intriguing and enigmatic phenomena in physics [1–3]. It signifies the nonclassical correlations between distinct quantum systems and has been applied in various fields, including quantum information processing [4,5], quantum communication [6–8], quantum precision measurements [9–11], and fundamental research in quantum mechanics [12–16]. Although uncertainties persist regarding the precise physical meaning of entanglement, numerous schemes have been proposed, both theoretical and experimental, to achieve entanglement in various physical systems, such as optomechanical systems [17–30], magnonic systems [31–39], and others [40,41].

In particular, the whispering-gallery-mode (WGM) resonator has been widely utilized, not only in research on entanglement generation, but also in various studies exploring other novel effects [42–60], owing to its distinctive optical characteristics. The WGM resonator possesses a high quality (Q) factor, naturally has two degenerate cavity modes [clockwise (CW) mode and counterclockwise (CCW) mode] with the same frequency, and can also support a mechanical breathing mode. However, backscattering induced by cavity imperfections, such as surface roughness or material defects, is also a noteworthy characteristic of the WGM resonator. This feature significantly suppresses various phenomena in the system, including intracavity photon number, optical transmission, optical chaos, optomechanical entanglement, mechanical squeezing, and system nonreciprocity [28–30,56–60]. Therefore, the identification of a feasible method to eliminate the impacts of backscattering becomes imperative. Recently, the revival of classical effects from backscattering has been experimentally achieved by introducing an additional nanotip or Mie scatter into the resonator [61,62].

Motivated by these abovementioned studies, herein, we present a general scheme to realize backscattering-immune optomechanical entanglement in the WGM optomechanical system by introducing an additional scatterer coupled with the WGM resonator. Meanwhile, we find that the classical information flow, referring to the transmissivity of the WGM resonator, can also be revived to the ideal case without backscattering. We also show that the robustness of the revived optomechanical entanglement against the cavity's dissipation and the mechanical thermal noise is enhanced [63]. Moreover, both the degree of optomechanical entanglement and the transmissivity can be manipulated by tuning the relative position of the introduced scatterer. This work provides insights into the protection and manipulation of quantum and classical resources. It is also universal [63] and can be compatible with other existing techniques, such as pump modulation [64–68], synthetic gauge fields [69], and dark-mode control [70–72]. These findings may

*Contact author: qguo@sxu.edu.cn

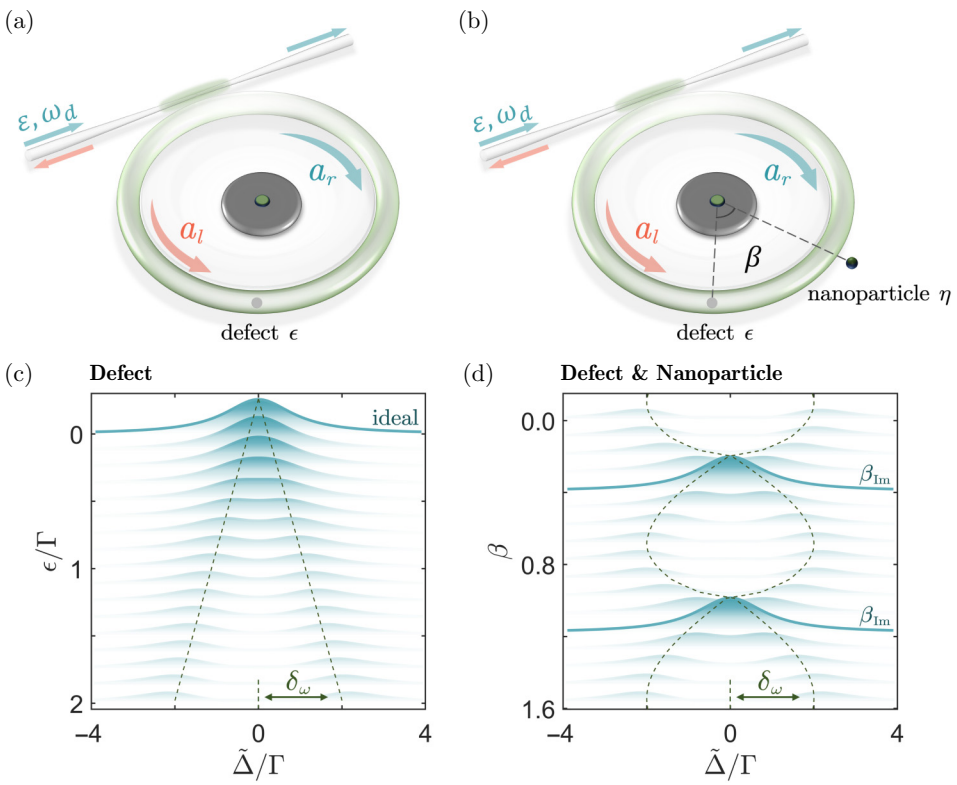

FIG. 1. (a) Schematic of the optomechanical system with a defect. Resonator with a defect is coupled to a tapered fiber through an evanescent field. Pump laser enters the fiber along the blue arrow to drive the CW mode. (b) Schematic of the backscattering-immune optomechanical system with a defect and nanoparticle. Nanoparticle is located in the evanescent field of the resonator with relative angle β. (c) Normalized intracavity mean photon number of the CW mode, $\mathcal{N}_r$, versus the effective optical detuning, $\tilde{\Delta}/\Gamma$, and backscattering strength, ϵ, in the system with a defect. $\delta_\omega = \Delta_\omega/2 = \sqrt{J_1 J_2}$ denotes half of the frequency splitting. (d) Normalized intracavity mean photon number of CW mode, N_r, versus effective optical detuning, $\tilde{\Delta}/\Gamma$, and relative angle, β, in the system with a defect and nanoparticle. See text for more parameters.

have potential applications in quantum information processing [73], quantum sensing [74], and the construction of quantum networks [75].

II. MODEL AND DYNAMICS

The theoretical model affected by the defect we consider is depicted in Fig. 1(a). It consists of two counterpropagating WGMs (a_r and a_l) with the same frequency (ω_c), and a mechanical breathing mode with frequency ω_m. The resonator is coupled with a tapered fiber through the evanescent field, and the fiber-cavity coupling rate is κ_{ex}. The CW mode of the resonator is driven by the laser with frequency ω_d fed into the fiber along the CW direction. Backscattering is induced by imperfections of the cavity, such as surface roughness or material defects, which can be approximated as a single scatterer because the coherence length of the circulating field is much longer than the cavity round-trip length [76]. We put another scatterer in the system to achieve the revival from backscattering, which can be realized by placing a nanoparticle in the evanescent field or defining a defect lithographically, and the effects of them are the same [62,77]. Here, we take the case of the nanoparticle as an example [Fig. 1(b)]. The interaction Hamiltonian between two optical modes is [78–80]

$$\hat{H}_J = \hbar J_1 \hat{a}_r^\dagger \hat{a}_l + \hbar J_2 \hat{a}_l^\dagger \hat{a}_r, \tag{1}$$

where $J_1 = \epsilon + \eta e^{-i2m\beta}$ and $J_2 = \epsilon + \eta e^{i2m\beta}$ are the backscattering rates caused by the defect and the nanoparticle, respectively; 2ϵ (2η) is the frequency splitting induced by the defect (nanoparticle) alone; the positive integer m is the azimuthal mode number, and we choose the experimental parameter [77] $m = 4$; β is the relative angle between the defect and the nanoparticle. The Hamiltonian of the system in the frame of $\hat{H}_0 = \hbar\omega_d \hat{a}_r^\dagger \hat{a}_r + \hbar\omega_d \hat{a}_l^\dagger \hat{a}_l$ is

$$\hat{H} = \hbar\Delta_c \hat{a}_r^\dagger \hat{a}_r + \hbar\Delta_c \hat{a}_l^\dagger \hat{a}_l + \hbar\frac{\omega_m}{2}(\hat{p}^2 + \hat{q}^2) + \hat{H}_J - \hbar G_0(\hat{a}_r^\dagger \hat{a}_r + \hat{a}_l^\dagger \hat{a}_l)\hat{q} + i\hbar\varepsilon(\hat{a}_r^\dagger - \hat{a}_r), \tag{2}$$

where $\hat{a}_{r(l)}$ is the photon-annihilation operator of the CW (CCW) mode; $\hat{q}(\hat{p})$ is the dimensionless mechanical displacement (momentum) operator for a mechanical breathing mode. $\Delta_c = \Delta_a + \Delta_J$; $\Delta_a = \omega_c - \omega_d$; $\Delta_J = \mathrm{Re}(\epsilon + \eta)$; and $G_0 = (\omega_c/R) \times \sqrt{\hbar/\mu\omega_m}$ denotes the single-photon cavity optomechanical (COM) coupling strength [81], with μ and R as the mass and radius of the resonator, respectively. $\varepsilon = \sqrt{2\kappa_{ex}} a_{\mathrm{in}}$, where $a_{\mathrm{in}} = \sqrt{P/\hbar\omega_d}$ is the amplitude of the input field and P is the input laser power. The defect and the nanoparticle only induce the frequency splitting of the optical modes, and the corresponding eigenfrequencies can be obtained from the Hamiltonian describing the optical modes and their interaction [63]: $\omega_{1,2} = \omega_c - i\Gamma + \epsilon + \eta \pm \sqrt{\epsilon^2 + \eta^2 + 2\epsilon\eta\cos(2m\beta)}$, where $\Gamma = \kappa_0 + \kappa_{ex}$ is the

total optical dissipation, and κ_0 is the intrinsic decay rate of the optical modes. The frequency splitting is $\Delta_\omega = \omega_1 - \omega_2 = 2\sqrt{J_1 J_2}$, as shown in Figs. 1(c) and 1(d), where the intracavity mean photon number of the CW mode reflects the cavity excitation spectrum, and the dashed lines refer to the eigenfrequencies versus ϵ and β. For the special case of $\beta = \beta_{\rm Im} \equiv \pi/8 + n\pi/4$ $(n \in \mathbb{Z})$, the eigenfrequency splitting, Δ_ω, is zero. To achieve backscattering immunity, we choose the parameters that are experimentally feasible with $\eta \sim \epsilon$ [62,77,82]: $\epsilon = \Gamma$ and $\eta = \Gamma$. For other parameter choices, backscattering revival (apart from the backscattering-immune case) also occurs and exhibits behavior similar to that shown in Fig. 1(d). When the dissipation and input noises are considered, the quantum Langevin equations of the system can be obtained:

$$\begin{aligned}
\dot{\hat{a}}_r &= (-i\Delta_c - \Gamma)\hat{a}_r - iJ_1\hat{a}_l + iG_0\hat{a}_r\hat{q} + \varepsilon \\
&\quad + \sqrt{2\kappa_0}\hat{a}^{\rm in}_{0,r} + \sqrt{2\kappa_{ex}}\hat{a}^{\rm in}_{ex,r}, \\
\dot{\hat{a}}_l &= (-i\Delta_c - \Gamma)\hat{a}_l - iJ_2\hat{a}_r + iG_0\hat{a}_l\hat{q} \\
&\quad + \sqrt{2\kappa_0}\hat{a}^{\rm in}_{0,l} + \sqrt{2\kappa_{ex}}\hat{a}^{\rm in}_{ex,l}, \\
\dot{\hat{q}} &= \omega_m\hat{p}, \\
\dot{\hat{p}} &= -\omega_m\hat{q} - \gamma_m\hat{p} + G_0(\hat{a}_r^\dagger\hat{a}_r + \hat{a}_l^\dagger\hat{a}_l) + \hat{\xi}, \qquad (3)
\end{aligned}$$

where γ_m is the mechanical decay rate, $\hat{a}^{\rm in}_{0,j}$ and $\hat{a}^{\rm in}_{ex,j}$ $(j = l, r)$ are the optical input vacuum noise operators, and $\hat{\xi}$ is the mechanical Brownian noise operator characterized by the following correlation functions [83,84]:

$$\begin{aligned}
&\langle \hat{a}^{\rm in}_{0(ex),j}(t)\hat{a}^{\rm in,\dagger}_{0(ex),j}(t')\rangle = \delta(t-t') \\
&\langle \hat{\xi}(t)\hat{\xi}(t')\rangle = \frac{\gamma_m}{\omega_m}\int \frac{d\omega}{2\pi} e^{-i\omega(t-t')}\omega\left[\coth\left(\frac{\hbar\omega}{2k_BT_e}\right)+1\right], \qquad (4)
\end{aligned}$$

where k_B is the Boltzmann constant and T_e is the environmental temperature. For the case where the mechanical oscillator has a high quality factor, $Q_m = \omega_m/\gamma_m \gg 1$; by using the Markovian approximation, the above correlation function of $\hat{\xi}(t)$ can be described as

$$\langle \hat{\xi}(t)\hat{\xi}(t')\rangle \approx \gamma_m(2n_m+1)\delta(t-t'), \qquad (5)$$

where $n_m = [\exp(\hbar\omega_m/k_BT_e) - 1]^{-1}$ is the mean thermal excitation phonon number.

Under the condition of strong optical driving, each operator can be expanded as a sum of its steady-state mean value and a small quantum fluctuation: $\hat{a}_j = \alpha_j + \delta\hat{a}_j$, $\hat{q} = q_s + \delta\hat{q}$, and $\hat{p} = p_s + \delta\hat{p}$, and the standard linearization techniques can be applied to the quantum Langevin equations in Eq. (3). By introducing quadrature operators

$$\begin{aligned}
&\delta\hat{X}_j = \frac{1}{\sqrt{2}}(\delta\hat{a}_j^\dagger + \delta\hat{a}_j), \quad \delta\hat{Y}_j = \frac{i}{\sqrt{2}}(\delta\hat{a}_j^\dagger - \delta\hat{a}_j), \\
&\hat{X}^{\rm in}_j = \sqrt{2\kappa_0}\hat{x}^{\rm in}_{0,j} + \sqrt{2\kappa_{ex}}\hat{x}^{\rm in}_{ex,j}, \quad \hat{x}^{\rm in}_j = \frac{1}{\sqrt{2}}(\delta\hat{a}^{\rm in\dagger}_j + \delta\hat{a}^{\rm in}_j), \\
&\hat{Y}^{\rm in}_j = \sqrt{2\kappa_0}\hat{y}^{\rm in}_{0,j} + \sqrt{2\kappa_{ex}}\hat{y}^{\rm in}_{ex,j}, \quad \hat{y}^{\rm in}_j = \frac{i}{\sqrt{2}}(\delta\hat{a}^{\rm in\dagger}_j - \delta\hat{a}^{\rm in}_j), \qquad (6)
\end{aligned}$$

and defining the column vectors of quadrature fluctuations and input noises as

$$\begin{aligned}
u^T &= (\delta\hat{X}_r, \delta\hat{Y}_r, \delta\hat{X}_l, \delta\hat{Y}_l, \delta\hat{q}, \delta\hat{p}), \\
v^T &= (\hat{X}^{\rm in}_r, \hat{Y}^{\rm in}_r, \hat{X}^{\rm in}_l, \hat{Y}^{\rm in}_l, 0, \hat{\xi}), \qquad (7)
\end{aligned}$$

we can rewrite the linearized quantum Langevin equations as

$$\dot{u}(t) = Au(t) + v(t), \qquad (8)$$

where

$$A = \begin{pmatrix}
-\Gamma & \tilde{\Delta} & \mathcal{J}_+ & \mathcal{J}_- & -G_r^y & 0 \\
-\tilde{\Delta} & -\Gamma & -\mathcal{J}_- & \mathcal{J}_+ & G_r^x & 0 \\
-\mathcal{J}_+ & \mathcal{J}_- & -\Gamma & \tilde{\Delta} & -G_l^y & 0 \\
-\mathcal{J}_- & -\mathcal{J}_+ & -\tilde{\Delta} & -\Gamma & G_l^x & 0 \\
0 & 0 & 0 & 0 & 0 & \omega_m \\
G_r^x & G_r^y & G_l^x & G_l^y & -\omega_m & -\gamma_m
\end{pmatrix}. \qquad (9)$$

Here, $\tilde{\Delta} = \Delta_c - G_0 q_s = \Delta + \Delta_J$ $(\Delta = \Delta_a - G_0 q_s)$ is the effective optical detuning, $a_{\rm in} = \sqrt{P/\hbar\omega_d} = \sqrt{P/\hbar(\omega_c - \Delta_a)} \simeq \sqrt{P/\hbar(\omega_c - \Delta)}$ (because of $\omega_d \gg G_0 q_s$), G_j^x (G_j^y) is the real (imaginary) part of the effective COM coupling rate, $G_j = \sqrt{2}G_0\alpha_j = G_j^x + iG_j^y$, $\mathcal{J}_+ = i(J_1 - J_2)/2 = \eta\sin 2m\beta$, and $\mathcal{J}_- = (J_1 + J_2)/2 = \epsilon + \eta\cos 2m\beta$. The steady-state mean values of the dynamical variables are

$$\begin{aligned}
&\alpha_r = \frac{(i\tilde{\Delta} + \Gamma)\varepsilon}{(i\tilde{\Delta}+\Gamma)^2 + J_1J_2}, \quad \alpha_l = \frac{-iJ_2\varepsilon}{(i\tilde{\Delta}+\Gamma)^2 + J_1J_2}, \\
&q_s = \frac{G_0}{\omega_m}(|\alpha_r|^2 + |\alpha_l|^2), \quad p_s = 0, \qquad (10)
\end{aligned}$$

and the intracavity photon numbers are $\mathcal{N}_j = |\alpha_j|^2$.

The solution of Eq. (8) is $u(t) = M(t)u(0) + \int_0^t d\tau M(t)v(t-\tau)$, where $M(t) = \exp(At)$. The system is stable and tends toward its steady state when all real parts of the eigenvalues of A are negative, resulting in $M(\infty) = 0$. The stability conditions can be derived based on the Routh-Hurwitz criterion [63,85]. If the system is stable, due to the linearized dynamics of quantum fluctuations

and the zero-mean Gaussian nature of quantum noise, the system will evolve into a Gaussian state independent of the initial state [86], and it can be completely described by the 6×6 covariance matrix, $V(t)$, with elements defined as $V_{kl}(t) = \langle u_k(t)u_l(t) + u_l(t)u_k(t)\rangle/2$. Then we can derive the motion equation of the covariance matrix, $\dot{V}(t) = A(t)V(t) + V(t)A^T(t) + D$, where the diffusion matrix is $D = \mathrm{Diag}[\Gamma, \Gamma, \Gamma, \Gamma, 0, (n_m + 1/2)\gamma_m]$. For the steady state, the motion equation of the covariance matrix becomes the Lyapunov equation [87]:

$$AV + VA^T = -D. \tag{11}$$

III. BACKSCATTERING-IMMUNE ENTANGLEMENT AND TRANSMISSION

By solving Eq. (11), we can obtain the covariance matrix, V. Extracting the two modes of interest and rewriting it in a 2×2 block form, we have

$$V' = \begin{pmatrix} \mathcal{A} & \mathcal{C} \\ \mathcal{C}^T & \mathcal{B} \end{pmatrix}, \tag{12}$$

and V' preserves the Gaussian nature. Then we can adopt the logarithmic negativity, $E_{\mathcal{N}}$, to quantify bipartite entanglement in the three-mode continuous-variable system [88], which is defined as [89]

$$E_{\mathcal{N}} = \max[0, -\ln(2\nu^-)], \tag{13}$$

where $\nu^- = 2^{-1/2}\{\sum(V') - [\sum(V')^2 - 4\det V']^{1/2}\}^{1/2}$; $\sum(V') = \det\mathcal{A} + \det\mathcal{B} - 2\det\mathcal{C}$. If, and only if, $\nu^- < 1/2$, the quantum bipartite entanglement exists, which is equivalent to Simon's necessary and sufficient entanglement criterion (or the related Peres-Horodecki criterion) for certifying the entanglement of the two-mode system in Gaussian states [90]. In COM, the driving laser is scattered by the mechanical mode into the Stokes and anti-Stokes sidebands. Optomechanical correlations are generated when either of these sidebands is resonant with the cavity, which is observed in experiments [23,24]. Here, we only consider the optomechanical entanglement for the case of the anti-Stokes sideband, i.e., the red-detuned driving field.

By using the input-output relationship [91], a_{out}=$a_{\mathrm{in}} - \sqrt{2\kappa_{ex}}\alpha_r$, which denotes the amplitude of the output field, the normalized transmission rate can be obtained [56]:

$$T = \left|\frac{a_{\mathrm{out}}}{a_{\mathrm{in}}}\right|^2 = \left|1 - \frac{2\kappa_{ex}(i\tilde{\Delta} + \Gamma)}{(i\tilde{\Delta} + \Gamma)^2 + J_1J_2}\right|^2. \tag{14}$$

Figure 2(a) shows the optomechanical entanglement, $E_{\mathcal{N},r}$, between the CW mode and the mechanical mode for different cases. The yellow dashed line denotes the ideal case without a defect, the red dotted-dashed line denotes the case of the cavity with a defect for $\epsilon = \Gamma$, and the blue solid line denotes the case of placing an appropriate nanoparticle (the backscattering rate induced by it is also Γ) at an angle of $\beta = \beta_{\mathrm{Im}}$. For the defective cavity, some photons are scattered from the CW mode to the CCW mode by the defect; this causes a reduction in the degree of optomechanical entanglement, $E_{\mathcal{N},r}$. By placing an appropriate nanoparticle in the evanescent field of the resonator with relative angle $\beta = \beta_{\mathrm{Im}}$, the degree of optomechanical entanglement, $E_{\mathcal{N},r}$, revives to the level of the ideal case without a defect, which means that backscattering immunity is achieved. The underlying physics of the revival from backscattering can be understood through destructive interference. The nanoparticle placed in the evanescent field of the WGM resonator will coherently scatter additional light from the pumped optical mode (CW mode) into the counterpropagating mode

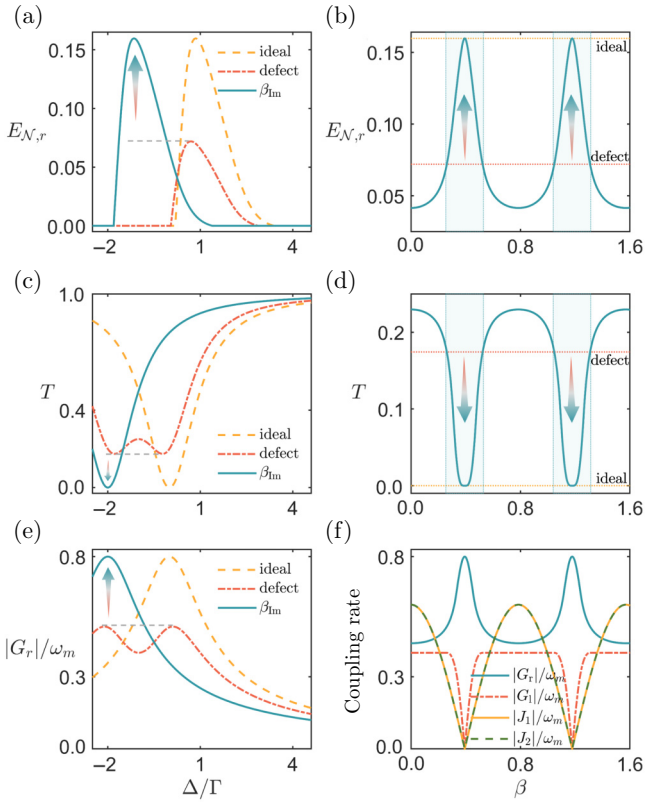

FIG. 2. (a) Optomechanical entanglement, $E_{\mathcal{N},r}$, versus Δ/Γ for different cases. (b) Maximum values of optomechanical entanglement, $E_{\mathcal{N},r}$, versus relative angle, β. Yellow dotted (red dotted) line denotes the maximum optomechanical entanglement between the CW mode and the mechanical mode without (with) the defect. (c) Normalized transmission rate, T, versus Δ/Γ for different cases. (d) Minimum normalized transmission, T, versus relative angle, β. (e) Effective COM coupling rate, $|G_r|/\omega_m$, versus Δ/Γ for different cases. (f) Maximum coupling rate versus relative angle, β. Backscattering immunity emerges for the angle $\beta = \beta_{\mathrm{Im}}$. See text for more parameters.

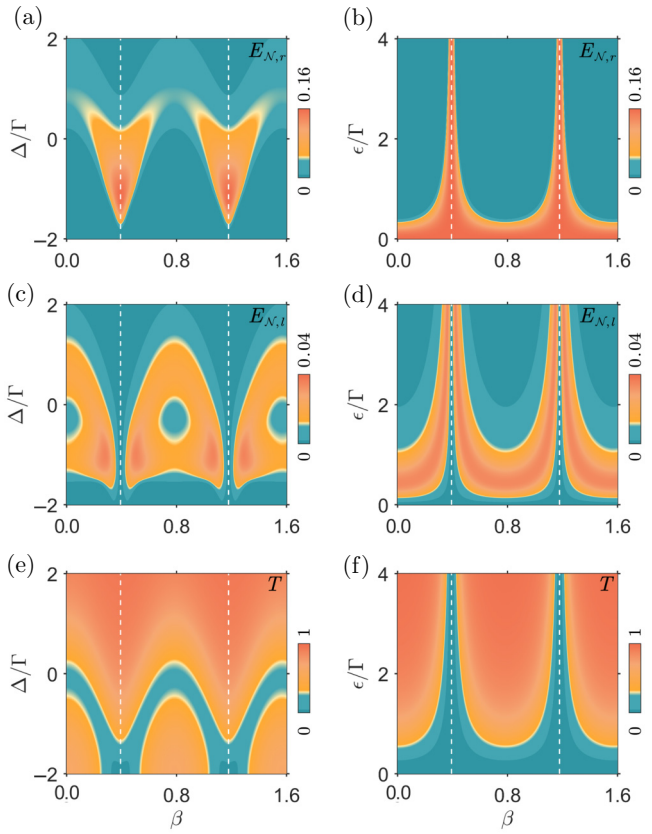

FIG. 3. (a) Optomechanical entanglement, $E_{\mathcal{N},r}$, versus relative angle, β, and Δ/Γ. (b) Optomechanical entanglement, $E_{\mathcal{N},r}$, versus relative angle, β, and ϵ/Γ for optimal detuning in (a) satisfying $\tilde{\Delta}/\Gamma = 0.85$. (c) Optomechanical entanglement, $E_{\mathcal{N},l}$, versus relative angle, β, and Δ/Γ. (d) Optomechanical entanglement, $E_{\mathcal{N},l}$, versus relative angle, β, and ϵ/Γ for the same detuning in (b). (e) Normalized transmission rate, T, versus relative angle, β, and Δ/Γ. (f) Normalized transmission rate, T, versus relative angle, β, and ϵ/Γ for optimal detuning in (e) satisfying $\tilde{\Delta}/\Gamma = 0$. Other parameters are the same as those in Fig. 2(a).

(CCW mode) to interfere with the backscattering light in CCW mode. Therefore, by adjusting the relative position and size of the nanoparticle properly, the defect-induced and scatterer-induced backpropagating fields can achieve perfect destructive interference, thus leading to the system's immunity to backscattering. In order to show the influence of the relative angle, β, on $E_{\mathcal{N},r}$, we plot the maximum values of optomechanical entanglement, $E_{\mathcal{N},r(l)}$, between the CW(CCW) mode and the mechanical mode versus the relative angle, β, in Fig. 2(b), which shows, as β varies, $E_{\mathcal{N},r}$ oscillates between the maximal entanglement in the ideal case and the one in the case with a defect. This means, for $\beta \neq \beta_{\mathrm{Im}}$, the revival of $E_{\mathcal{N},r}$ also exists (blue region), but backscattering immunity only emerges at an angle of $\beta = \beta_{\mathrm{Im}}$. We plot the transmission rate, T, versus Δ/Γ in Fig. 2(c) for the three cases, similarly to

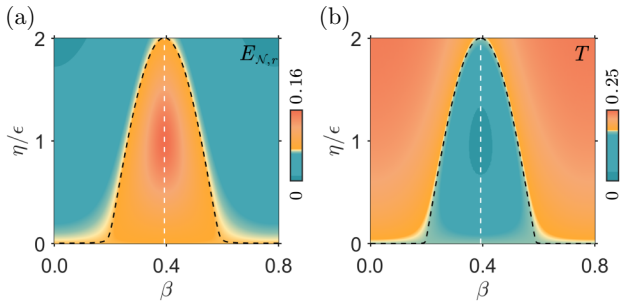

FIG. 4. (a) Maximum optomechanical entanglement, $E_{\mathcal{N},r}$, versus relative angle, β, and η/ϵ. (b) Minimum normalized transmission rate, T, versus relative angle, β, and η/ϵ. Black dashed lines denote the case with a defect and without a nanoparticle. Other parameters are the same as those in Fig. 2(a).

Fig. 2(a), which shows that the transmission-rate curve for the defective cavity can also be restored to be the same as that in the ideal case, besides a frequency shift by placing a nanoparticle at an angle of $\beta = \beta_{\mathrm{Im}}$. Figure 2(d) exhibits the influence of β on the dip of the transmission-rate curve. To better understand the revival, we plot the effective COM coupling rate, $|G_r|$, versus Δ/Γ for the same three cases in Fig. 2(e), and the maximum coupling rate, $|G_{r(l)}|$, and the backscattering rate, $|J_{1(2)}|$, versus relative angle, β, in Fig. 2(f). Comparing Fig. 2(e) with Figs. 2(a) and 2(c), one can see that the revival of the entanglement and transmission rate is attributed to the revival of the effective COM coupling rate. From Fig. 2(f), the decrease of the backscattering rate, $|J_{1(2)}|$, causes the increase of $|G_r|$ and the decrease of $|G_l|$. For the case of $\beta = \beta_{\mathrm{Im}}$, the CW mode is decoupled from the CCW mode, that is, the effect of backscattering is eliminated, which means the system revives to the ideal system without a defect (except the frequency shift caused by scatterers). More importantly, this point is a "sweet spot." Specifically, based on the first and second derivatives of $J_{1(2)}$ ($|\dot{J}_{1(2)}(\beta)| = -(2m\epsilon\eta\sin(2m\beta)/\sqrt{\epsilon^2+\eta^2+2\epsilon\eta\cos(\pm 2m\beta)})$, $|\ddot{J}_{1(2)}(\beta)| = -(4m^2\epsilon\eta[\cos(2m\beta)(\epsilon^2+\eta^2+2\epsilon\eta\cos(2m\beta))+\epsilon\eta\sin^2(2m\beta)]/(\epsilon^2+\eta^2+2\epsilon\eta\cos(2m\beta))^{3/2})$), we find that, regardless of other parameter values, when $\beta = \beta_{\mathrm{Im}}$, $|\dot{J}_{1(2)}(\beta)| = 0$ and $|\ddot{J}_{1(2)}(\beta)| > 0$, i.e., the backscattering rate reaches its minimum value. Furthermore, under the condition $\eta < 2\epsilon$, backscattering suppression occurs (which we prove later). The parameters we choose are experimentally feasible to ensure the stability of the system [92,93]: $\mu = 10$ ng, $R = 1.1 \times 10^{-3}$ m, $T_e = 200$ mK, $\omega_m = 63 \times 10^6$ Hz, $\gamma_m = 10^{-5}\omega_m$, $\omega_c = 1.22 \times 10^{15}$ Hz, $\kappa_0 = 0.3\omega_m$, κ_{ex}=κ_0, and $P = 30$ mW.

To exhibit the parameter regions for the revival and backscattering immunity clearly, we plot $E_{\mathcal{N},r}$, $E_{\mathcal{N},l}$, and T versus the relative angle, β, and Δ/Γ in Figs. 3(a), 3(c), and 3(e), respectively, where the white dotted lines denote the backscattering-immune angle, $\beta = \beta_{\mathrm{Im}}$. We can see the

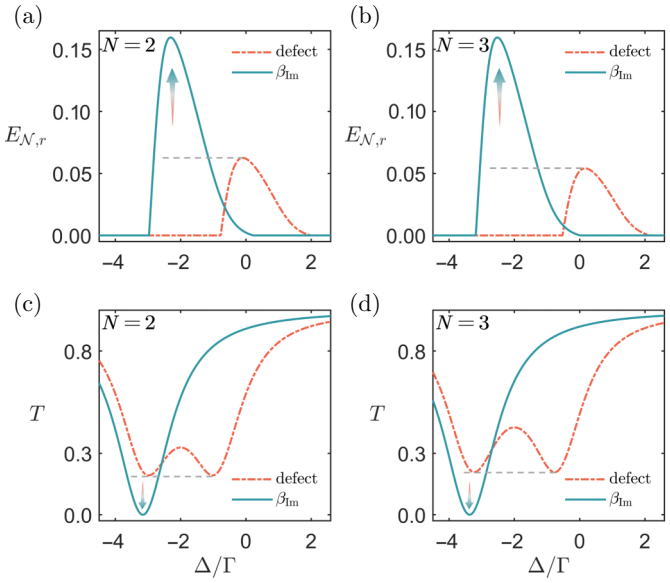

FIG. 5. (a),(b) Backscattering-immune optomechanical entanglement, $E_{\mathcal{N},r}$; and (c),(d) backscattering-immune normalized transmission, T, versus Δ/Γ with multiple defects. (a),(c) Defect number $N=2$; (b),(d) $N=3$. Here, $\sum_j \epsilon_j = 2\Gamma$, $\beta_j = \mathcal{R}_{\beta_j}$, and other parameters are the same as those in Fig. 2(a).

degree of optomechanical entanglement and the transmission rate are changed by tuning the relative angle of the nanoparticle, which not only means we can manipulate the entanglement and transmission by tuning the position of the nanoparticle, but also the scheme has the potential to be used for nanoparticle sensing. We also plot the revival for different backscattering strengths, ϵ, in Figs. 3(b), 3(d), and 3(f), which show that backscattering immunity still emerges at $\beta = \beta_{\rm Im}$ for large values of ϵ. However, the angle region for the revival decreases as ϵ increases, which means, for strong backscattering, backscattering immunity requires the position of the nanoparticle to be sufficiently precise. We have chosen $\eta = \epsilon$ in the above analysis. In Figs. 4(a) and 4(b), we show the revival of $E_{\mathcal{N},r}$ and T from backscattering versus different relative angles, β, and different η; this reflects the revival's tolerance for the position and size of the nanoparticle. The black dashed lines denote the degree in the case with a defect and without a nanoparticle; therefore, the region under the black dashed line denote the region with revival from backscattering. The big revival region means the scheme is robust against the size of the nanoparticle and the manipulation accuracy of the nanoparticle.

The scheme can also be generalized to the case of multiple defects. By placing an appropriate nanoparticle, backscattering immunity can be achieved. For this case, the backscattering rate is $J_{1(2)} = \sum_j \epsilon_j e^{\mp i2m\beta_j} + \eta e^{\mp i2m\beta}$. The terms originating from defects can be directly written as a single scatterer: $\sum_j \epsilon_j e^{\mp i2m\beta_j} \Rightarrow \epsilon' e^{\mp i2m\beta'}$, where $\epsilon' = |\sum_j \epsilon_j e^{\mp i2m\beta_j}|$ and $2m\beta' = \arg(\sum_j \epsilon_j e^{i2m\beta_j})$. By adjusting the nanoparticle to $\eta = \epsilon'$ and $\beta = \beta' + \beta_{\rm Im}$, the back-propagating fields achieve perfect destructive interference, leading to backscattering immunity. Figure 5 illustrates the revival from backscattering for different numbers, N, of defects; the backscattering-immune entanglement [Figs. 5(a) and 5(b)] and transmission [Figs. 5(c) and 5(d)] emerge, as we analyzed above. Here, we maintain $\sum_j \epsilon_j = 2\Gamma$ and choose random parameters to ensure the universality of the results: the relative angles of scatterers are $\beta_j = \mathcal{R}_{\beta_j}$ and $\epsilon_j = \mathcal{R}_{\epsilon_j}$, where $\mathcal{R}$ denotes a randomly generated real number and its subscript corresponds to the specific parameter. Furthermore, we demonstrate that the optomechanical entanglement, $E_{\mathcal{N},r}$, can survive even when it is fully destroyed by thermal noise and dissipation in the device with a defect, and some other effects in the system also exhibit similar revival behavior against backscattering [63,94].

IV. CONCLUSION

We have shown how to achieve backscattering immunity in a defective whispering-gallery cavity device by placing a nanoparticle in the evanescent field of the resonator, and we demonstrated that the revival of $E_{\mathcal{N},r}$ and T from backscattering was robust against the position and size of the nanoparticle. Furthermore, one can control the optomechanical entanglement and transmission by tuning the relative position of the nanoparticle. We also generalized the scheme for the case of multiple defects in the cavity. This work provides a new way to protect and manipulate the quantum and classical source effectively in the quantum system containing an imperfect whispering-gallery-mode cavity, which may be widely applied in the field of quantum technology, such as in quantum processors, quantum sensing, and quantum precision measurements.

ACKNOWLEDGMENTS

This work was supported by the National Natural Science Foundation of China under Grant No. 12274274.

DATA AVAILABILITY

The data supporting the results of this study are available from the corresponding author upon reasonable request.

[1] E. Schrödinger, Discussion of probability relations between separated systems, Math. Proc. Cambridge **31**, 555 (1935).
[2] A. Einstein, B. Podolsky, and N. Rosen, Can quantum-mechanical description of physical reality be considered complete? Phys. Rev. **47**, 777 (1935).

[3] R. Horodecki, P. Horodecki, M. Horodecki, and K. Horodecki, Quantum entanglement, Rev. Mod. Phys. **81**, 865 (2009).

[4] U. Andersen, G. Leuchs, and C. Silberhorn, Continuous-variable quantum information processing, Laser Photonics Rev. **4**, 337 (2010).

[5] F. Flamini, N. Spagnolo, and F. Sciarrino, Photonic quantum information processing: A review, Rep. Prog. Phys. **82**, 016001 (2018).

[6] R. Ursin, F. Tiefenbacher, T. Schmitt-Manderbach, H. Weier, T. Scheidl, M. Lindenthal, B. Blauensteiner, T. Jennewein, J. Perdigues, P. Trojek, B. Ömer, M. Fürst, M. Meyenburg, J. Rarity, Z. Sodnik, C. Barbieri, H. Weinfurter, and A. Zeilinger, Entanglement-based quantum communication over 144 km, Nat. Phys. **3**, 481 (2007).

[7] J.-W. Pan, C. Simon, Č. Brukner, and A. Zeilinger, Entanglement purification for quantum communication, Nature (London) **410**, 1067 (2001).

[8] Q. Guo, L.-Y. Cheng, L. Chen, H.-F. Wang, and S. Zhang, Counterfactual quantum-information transfer without transmitting any physical particles, Sci. Rep. **5**, 8416 (2015).

[9] H. Yu, L. McCuller, M. Tse, N. Kijbunchoo, L. Barsotti, and N. Mavalvala, COLLABL. S. Collaboration.Quantum correlations between light and the kilogram-mass mirrors of LIGO, Nature (London) **583**, 43 (2020).

[10] M. D. LaHaye, O. Buu, B. Camarota, and K. C. Schwab, Approaching the quantum limit of a nanomechanical resonator, Science **304**, 74 (2004).

[11] A. Motazedifard, F. Bemani, M. H. Naderi, R. Roknizadeh, and D. Vitali, Force sensing based on coherent quantum noise cancellation in a hybrid optomechanical cavity with squeezed-vacuum injection, New J. Phys. **18**, 073040 (2016).

[12] M. Giustina, *et al.*, Significant-loophole-free test of Bell's theorem with entangled photons, Phys. Rev. Lett. **115**, 250401 (2015).

[13] L. K. Shalm, *et al.*, Strong loophole-free test of local realism, Phys. Rev. Lett. **115**, 250402 (2015).

[14] B. Hensen, H. Bernien, A. E. Dréau, A. Reiserer, N. Kalb, M. S. Blok, J. Ruitenberg, R. F. L. Vermeulen, R. N. Schouten, C. Abellán, W. Amaya, V. Pruneri, M. W. Mitchell, M. Markham, D. J. Twitchen, D. Elkouss, S. Wehner, T. H. Taminiau, and R. Hanson, Loophole-free Bell inequality violation using electron spins separated by 1.3 kilometres, Nature (London) **526**, 682 (2015).

[15] F.-X. Sun, S.-S. Zheng, Y. Xiao, Q. Gong, Q. He, and K. Xia, Remote generation of magnon Schrödinger cat state via magnon-photon entanglement, Phys. Rev. Lett. **127**, 087203 (2021).

[16] D. Han, F. Sun, N. Wang, Y. Xiang, M. Wang, M. Tian, Q. He, and X. Su, Remote preparation of optical cat states based on Gaussian entanglement, Laser Photonics Rev. **17**, 2300103 (2023).

[17] Y.-D. Wang and A. A. Clerk, Reservoir-engineered entanglement in optomechanical systems, Phys. Rev. Lett. **110**, 253601 (2013).

[18] Y.-D. Wang, S. Chesi, and A. A. Clerk, Bipartite and tripartite output entanglement in three-mode optomechanical systems, Phys. Rev. A **91**, 013807 (2015).

[19] Z.-Y. Fan, H. Qian, X. Zuo, and J. Li, Entangling ferrimagnetic magnons with an atomic ensemble via optomagnomechanics, Phys. Rev. A **108**, 023501 (2023).

[20] Q. Guo, M.-R. Wei, C.-H. Bai, Y. Zhang, G. Li, and T. Zhang, Manipulation and enhancement of Einstein-Podolsky-Rosen steering between two mechanical modes generated by two Bogoliubov dissipation pathways, Phys. Rev. Res. **5**, 013073 (2023).

[21] W.-J. Zhang, Y. Zhang, Q. Guo, A.-Peng Liu, G. Li, and T. Zhang, Strong mechanical squeezing and optomechanical entanglement in a dissipative double-cavity system via pump modulation, Phys. Rev. A **104**, 053506 (2021).

[22] R. Riedinger, A. Wallucks, I. Marinković, C. Löschnauer, M. Aspelmeyer, S. Hong, and S. Gröblacher, Remote quantum entanglement between two micromechanical oscillators, Nature (London) **556**, 473 (2018).

[23] R. Riedinger, S. Hong, R. A. Norte, J. A. Slater, J. Shang, A. G. Krause, V. Anant, M. Aspelmeyer, and S. Gröblacher, Non-classical correlations between single photons and phonons from a mechanical oscillator, Nature (London) **530**, 313 (2016).

[24] T. A. Palomaki, J. D. Teufel, R. W. Simmonds, and K. W. Lehnert, Entangling mechanical motion with microwave fields, Science **342**, 710 (2013).

[25] C. F. Ockeloen-Korppi, E. Damskägg, J.-M. Pirkkalainen, M. Asjad, A. A. Clerk, F. Massel, M. J. Woolley, and M. A. Sillanpää, Stabilized entanglement of massive mechanical oscillators, Nature (London) **556**, 478 (2018).

[26] J. M. Raimond, M. Brune, and S. Haroche, Manipulating quantum entanglement with atoms and photons in a cavity, Rev. Mod. Phys. **73**, 565 (2001).

[27] S.-X. Wu, C.-H. Bai, G. Li, C. shui Yu, and T. Zhang, Quantum squeezing-induced quantum entanglement and EPR steering in a coupled optomechanical system, Opt. Express **32**, 260 (2024).

[28] Y.-F. Jiao, S.-D. Zhang, Y.-L. Zhang, A. Miranowicz, L.-M. Kuang, and H. Jing, Nonreciprocal optomechanical entanglement against backscattering losses, Phys. Rev. Lett. **125**, 143605 (2020).

[29] Y.-F. Jiao, J.-X. Liu, Y. Li, R. Yang, L.-M. Kuang, and H. Jing, Nonreciprocal enhancement of remote entanglement between nonidentical mechanical oscillators, Phys. Rev. Appl. **18**, 064008 (2022).

[30] J.-X. Liu, Y.-F. Jiao, Y. Li, X.-W. Xu, Q.-Y. He, and H. Jing, Phase-controlled asymmetric optomechanical entanglement against optical backscattering, Sci. China Phys. Mech. Astron. **66**, 230312 (2023).

[31] J. Li, S.-Y. Zhu, and G. S. Agarwal, Magnon-photon-phonon entanglement in cavity magnomechanics, Phys. Rev. Lett. **121**, 203601 (2018).

[32] M. Yu, H. Shen, and J. Li, Magnetostrictively induced stationary entanglement between two microwave fields, Phys. Rev. Lett. **124**, 213604 (2020).

[33] Z.-Y. Fan, L. Qiu, S. Gröblacher, and J. Li, Microwave-optics entanglement via cavity optomagnomechanics, Laser Photonics Rev. **17**, 2200866 (2023).

[34] J. Li and S. Gröblacher, Entangling the vibrational modes of two massive ferromagnetic spheres using cavity magnomechanics, Quantum Sci. Technol. **6**, 024005 (2021).

[35] Z.-Y. Fan, H. Qian, and J. Li, Stationary optomagnonic entanglement and magnon-to-optics quantum state transfer via opto-magnomechanics, Quantum Sci. Technol. **8**, 015014 (2022).
[36] H. Qian, Z.-Y. Fan, and J. Li, Entangling mechanical vibrations of two massive ferrimagnets by fully exploiting the nonlinearity of magnetostriction, Quantum Sci. Technol. **8**, 015022 (2022).
[37] S. Chakraborty and C. Das, Nonreciprocal magnon-photon-phonon entanglement in cavity magnomechanics, Phys. Rev. A **108**, 063704 (2023).
[38] Y. long Ren, Nonreciprocal optical–microwave entanglement in a spinning magnetic resonator, Opt. Lett. **47**, 1125 (2022).
[39] Z.-B. Yang, J.-S. Liu, A.-D. Zhu, H.-Y. Liu, and R.-C. Yang, Nonreciprocal transmission and nonreciprocal entanglement in a spinning microwave magnomechanical system, Ann. Phys. **532**, 2000196 (2020).
[40] J. Li and S. Gröblacher, Stationary quantum entanglement between a massive mechanical membrane and a low frequency *LC* circuit, New J. Phys. **22**, 063041 (2020).
[41] A. Stute, B. Casabone, P. Schindler, T. Monz, P. O. Schmidt, B. Brandstätter, T. E. Northup, and R. Blatt, Tunable ion–photon entanglement in an optical cavity, Nature (London) **485**, 482 (2012).
[42] W. Chen, Ş. Kaya Özdemir, G. Zhao, J. Wiersig, and L. Yang, Exceptional points enhance sensing in an optical microcavity, Nature (London) **548**, 192 (2017).
[43] B. Zhao, K.-X. Zhou, M.-R. Wei, J. Cao, and Q. Guo, Nonreciprocal strong mechanical squeezing based on the Sagnac effect and two-tone driving, Opt. Lett. **49**, 486 (2024).
[44] H. Lü, C. Wang, L. Yang, and H. Jing, Optomechanically induced transparency at exceptional points, Phys. Rev. Appl. **10**, 014006 (2018).
[45] R. Huang, A. Miranowicz, J.-Q. Liao, F. Nori, and H. Jing, Nonreciprocal photon blockade, Phys. Rev. Lett. **121**, 153601 (2018).
[46] R. Huang, K. Özdemir, J.-Q. Liao, F. Minganti, L.-M. Kuang, F. Nori, and H. Jing, Exceptional photon blockade: Engineering photon blockade with chiral exceptional points, Laser Photonics Rev. **16**, 2100430 (2022).
[47] Y. Chen, Y.-L. Zhang, Z. Shen, C.-L. Zou, G.-C. Guo, and C.-H. Dong, Synthetic gauge fields in a single optomechanical resonator, Phys. Rev. Lett. **126**, 123603 (2021).
[48] Z. Shen, Y.-L. Zhang, Y. Chen, Y.-F. Xiao, C.-L. Zou, G.-C. Guo, and C.-H. Dong, Nonreciprocal frequency conversion and mode routing in a microresonator, Phys. Rev. Lett. **130**, 013601 (2023).
[49] J. Li, Y.-P. Wang, W.-J. Wu, S.-Y. Zhu, and J.-Q. You, Quantum network with magnonic and mechanical nodes, PRX Quantum **2**, 040344 (2021).
[50] D. Cheng, K. Wang, and S. Fan, Artificial non-Abelian lattice gauge fields for photons in the synthetic frequency dimension, Phys. Rev. Lett. **130**, 083601 (2023).
[51] Y.-l. Ren, S.-l. Ma, J.-k. Xie, X.-k. Li, M.-t. Cao, and F.-l. Li, Nonreciprocal single-photon quantum router, Phys. Rev. A **105**, 013711 (2022).
[52] Z. Shen, Y.-L. Zhang, C.-L. Zou, G.-C. Guo, and C.-H. Dong, Dissipatively controlled optomechanical interaction via cascaded photon-phonon coupling, Phys. Rev. Lett. **126**, 163604 (2021).
[53] J.-S. Tang, W. Nie, L. Tang, M. Chen, X. Su, Y. Lu, F. Nori, and K. Xia, Nonreciprocal single-photon band structure, Phys. Rev. Lett. **128**, 203602 (2022).
[54] F. Zhang, Y. Feng, X. Chen, L. Ge, and W. Wan, Synthetic anti-PT symmetry in a single microcavity, Phys. Rev. Lett. **124**, 053901 (2020).
[55] Y. Zheng, J. Yang, Z. Shen, J. Cao, X. Chen, X. Liang, and W. Wan, Optically induced transparency in a micro-cavity, Light Sci. Appl. **5**, e16072 (2016).
[56] H. Jing, H. Lü, S. K. Özdemir, T. Carmon, and F. Nori, Nanoparticle sensing with a spinning resonator, Optica **5**, 1424 (2018).
[57] H. Zhang, R. Huang, S.-D. Zhang, Y. Li, C.-W. Qiu, F. Nori, and H. Jing, Breaking anti-PT symmetry by spinning a resonator, Nano Lett. **20**, 7594 (2020).
[58] Q. Guo, K.-X. Zhou, C.-H. Bai, Y. Zhang, G. Li, and T. Zhang, Nonreciprocal mechanical squeezing in a spinning cavity optomechanical system via pump modulation, Phys. Rev. A **108**, 033515 (2023).
[59] D.-W. Zhang, L.-L. Zheng, C. You, C.-S. Hu, Y. Wu, and X.-Y. Lü, Nonreciprocal chaos in a spinning optomechanical resonator, Phys. Rev. A **104**, 033522 (2021).
[60] Z.-Y. Fan, X. Zuo, H.-T. Li, and J. Li, Nonreciprocal entanglement in cavity magnomechanics exploiting chiral cavity-magnon coupling, arXiv:2401.02280.
[61] A. Ø. Svela, J. M. Silver, L. Del Bino, S. Zhang, M. T. M. Woodley, M. R. Vanner, and P. Del'Haye, Coherent suppression of backscattering in optical microresonators, Light Sci. Appl. **9**, 204 (2020).
[62] H. Lee, A. Kecebas, F. Wang, L. Chang, S. K. Özdemir, and T. Gu, Chiral exceptional point and coherent suppression of backscattering in silicon microring with low loss Mie scatterer, eLight **3**, 20 (2023).
[63] See the Supplemental Material at http://link.aps.org/supplemental/10.1103/PhysRevApplied.23.024061 for a detailed discussion of eigenfrequency calculations, system-stability analysis, robustness enhancement against environmental temperature and optical dissipation, backscattering-immune intracavity photon number and EPR steering, and revival from backscattering in the non-Hermitian case.
[64] A. Mari and J. Eisert, Gently modulating optomechanical systems, Phys. Rev. Lett. **103**, 213603 (2009).
[65] M. R. Vanner, I. Pikovski, G. D. Cole, M. S. Kim, Brukner, K. Hammerer, G. J. Milburn, and M. Aspelmeyer, Pulsed quantum optomechanics, Proc. Natl. Acad. Sci. USA **108**, 16182 (2011).
[66] S. M. Meenehan, J. D. Cohen, G. S. MacCabe, F. Marsili, M. D. Shaw, and O. Painter, Pulsed excitation dynamics of an optomechanical crystal resonator near its quantum ground state of motion, Phys. Rev. X **5**, 041002 (2015).
[67] Q. Guo, X.-Q. Ren, C.-H. Bai, Y. Zhang, G. Li, and T. Zhang, Mechanical squeezing in an active-passive-coupled double-cavity optomechanical system via pump modulation, Opt. Express **30**, 47070 (2022).
[68] Y.-H. Liu, Y. Zeng, Q.-S. Tan, D. Dong, F. Nori, and J.-Q. Liao, Optimal control of linear Gaussian quantum systems via quantum learning control, Phys. Rev. A **109**, 063508 (2024).

[69] D.-G. Lai, J.-Q. Liao, A. Miranowicz, and F. Nori, Noise-tolerant optomechanical entanglement via synthetic magnetism, Phys. Rev. Lett. **129**, 063602 (2022).
[70] D.-G. Lai, F. Zou, B.-P. Hou, Y.-F. Xiao, and J.-Q. Liao, Simultaneous cooling of coupled mechanical resonators in cavity optomechanics, Phys. Rev. A **98**, 023860 (2018).
[71] J. Huang, D.-G. Lai, and J.-Q. Liao, Controllable generation of mechanical quadrature squeezing via dark-mode engineering in cavity optomechanics, Phys. Rev. A **108**, 013516 (2023).
[72] Q. Guo, J. Cao, C.-H. Bai, Y. Zhang, G. Li, and T. Zhang, Asymmetrical simultaneous squeezing of multiple mechanical oscillators via synthetic magnetism, Phys. Rev. A **108**, 053512 (2023).
[73] K. Stannigel, P. Komar, S. J. M. Habraken, S. D. Bennett, M. D. Lukin, P. Zoller, and P. Rabl, Optomechanical quantum information processing with photons and phonons, Phys. Rev. Lett. **109**, 013603 (2012).
[74] Y. Ma, H. Miao, B. H. Pang, M. Evans, C. Zhao, J. Harms, R. Schnabel, and Y. Chen, Proposal for gravitational-wave detection beyond the standard quantum limit through EPR entanglement, Nat. Phys. **13**, 776 (2017).
[75] T.-X. Lu, B. Li, Y. Wang, D.-Y. Wang, X. Xiao, and H. Jing, Directional quantum-squeezing-enabled nonreciprocal enhancement of entanglement, Phys. Rev. Appl. **22**, 064001 (2024).
[76] J. Matres and W. V. Sorin, Simple model for ring resonators backscatter, Opt. Express **25**, 3242 (2017).
[77] B. Peng, Şahin Kaya Özdemir, M. Liertzer, W. Chen, J. Kramer, H. Yılmaz, J. Wiersig, S. Rotter, and L. Yang, Chiral modes and directional lasing at exceptional points, Proc. Natl. Acad. Sci. USA **113**, 6845 (2016).
[78] J. Hou, J. Lin, J. Zhu, G. Zhao, Y. Chen, F. Zhang, Y. Zheng, X. Chen, Y. Cheng, L. Ge, and W. Wan, Self-induced transparency in a perfectly absorbing chiral second-harmonic generator, PhotoniX **3**, 22 (2022).
[79] J. Wiersig, S. W. Kim, and M. Hentschel, Asymmetric scattering and nonorthogonal mode patterns in optical microspirals, Phys. Rev. A **78**, 053809 (2008).
[80] J. Qie, C. Wang, and L. Yang, Chirality induced nonreciprocity in a nonlinear optical microresonator, Laser Photonics Rev. **17**, 2200717 (2023).
[81] M. Aspelmeyer, T. J. Kippenberg, and F. Marquardt, Cavity optomechanics, Rev. Mod. Phys. **86**, 1391 (2014).
[82] S. Kim, J. M. Taylor, and G. Bahl, Dynamic suppression of Rayleigh backscattering in dielectric resonators, Optica **6**, 1016 (2019).
[83] C. Gardiner and P. Zoller, *Quantum Noise* (Springer Science & Business Media, Berlin, 2004).
[84] V. Giovannetti and D. Vitali, Phase-noise measurement in a cavity with a movable mirror undergoing quantum Brownian motion, Phys. Rev. A **63**, 023812 (2001).
[85] E. X. DeJesus and C. Kaufman, Routh-Hurwitz criterion in the examination of eigenvalues of a system of nonlinear ordinary differential equations, Phys. Rev. A **35**, 5288 (1987).
[86] C. Weedbrook, S. Pirandola, R. García-Patrón, N. J. Cerf, T. C. Ralph, J. H. Shapiro, and S. Lloyd, Gaussian quantum information, Rev. Mod. Phys. **84**, 621 (2012).
[87] D. Vitali, S. Gigan, A. Ferreira, H. R. Böhm, P. Tombesi, A. Guerreiro, V. Vedral, A. Zeilinger, and M. Aspelmeyer, Optomechanical entanglement between a movable mirror and a cavity field, Phys. Rev. Lett. **98**, 030405 (2007).
[88] G. Vidal and R. F. Werner, Computable measure of entanglement, Phys. Rev. A **65**, 032314 (2002).
[89] G. Adesso, A. Serafini, and F. Illuminati, Extremal entanglement and mixedness in continuous variable systems, Phys. Rev. A **70**, 022318 (2004).
[90] R. Simon, Peres-Horodecki separability criterion for continuous variable systems, Phys. Rev. Lett. **84**, 2726 (2000).
[91] C. W. Gardiner and M. J. Collett, Input and output in damped quantum systems: Quantum stochastic differential equations and the master equation, Phys. Rev. A **31**, 3761 (1985).
[92] G. C. Righini, Y. Dumeige, P. Féron, M. Ferrari, G. Nunzi Conti, D. Ristic, and S. Soria, Whispering gallery mode microresonators: Fundamentals and applications, Riv. Nuovo Cimento **34**, 435 (2011).
[93] S. Maayani, R. Dahan, Y. Kligerman, E. Moses, A. U. Hassan, H. Jing, F. Nori, D. N. Christodoulides, and T. Carmon, Flying couplers above spinning resonators generate irreversible refraction, Nature (London) **558**, 569 (2018).
[94] I. Kogias, A. R. Lee, S. Ragy, and G. Adesso, Quantification of Gaussian quantum steering, Phys. Rev. Lett. **114**, 060403 (2015).